Science Bulletin xxx (xxxx) xxx

Contents lists available at ScienceDirect

Science Bulletin

journal homepage: www.elsevier.com/locate/scib

Article

Iontronic pressure sensor with high sensitivity and linear response over a wide pressure range based on soft micropillared electrodes

Peng Lu [a], Liu Wang [a], Pang Zhu [a], Jun Huang [a], Yueji Wang [a], Ningning Bai [a], Yan Wang [a], Gang Li [a], Junlong Yang [a], Kewei Xie [a], Jianming Zhang [b], Bo Yu [c], Yuan Dai [d], Chuan Fei Guo [a,e,*]

[a] Department of Materials Science and Engineering, Southern University of Science and Technology, Shenzhen 518055, China
[b] Academy for Advanced Interdisciplinary Studies, Southern University of Science and Technology, Shenzhen 518055, China
[c] Ningbo Fengcheng Advanced Energy Materials Research Institute, Ningbo 315500, China
[d] Tencent Robotics X, Shenzhen 518000, China
[e] Centers for Mechanical Engineering Research and Education at MIT and SUSTech & Shenzhen Engineering Research Center for Novel Electronic Information Materials and Devices, Southern University of Science and Technology, Shenzhen 518055, China

ARTICLE INFO

Article history:
Received 1 December 2020
Received in revised form 14 January 2021
Accepted 29 January 2021
Available online xxxx

Keywords:
Iontronic interface
Linearity
Flexible pressure sensor
Mechanical matching

ABSTRACT

Electronic skins and flexible pressure sensors are important devices for advanced healthcare and intelligent robotics. Sensitivity is a key parameter of flexible pressure sensors. Whereas introducing surface microstructures in a capacitive-type sensor can significantly improve its sensitivity, the signal becomes nonlinear and the pressure response range gets much narrower, significantly limiting the applications of flexible pressure sensors. Here, we designed a pressure sensor that utilizes a nanoscale iontronic interface of an ionic gel layer and a micropillared electrode, for highly linear capacitance-to-pressure response and high sensitivity over a wide pressure range. The micropillars undergo three stages of deformation upon loading: initial contact (0–6 kPa) and structure buckling (6–12 kPa) that exhibit a low and nonlinear response, as well as a post-buckling stage that has a high signal linearity with high sensitivity (33.16 kPa^{-1}) over a broad pressure range of 12–176 kPa. The high linearity lies in the subtle balance between the structure compression and mechanical matching of the two materials at the gel-electrode interface. Our sensor has been applied in pulse detection, plantar pressure mapping, and grasp task of an artificial limb. This work provides a physical insight in achieving linear response through the design of appropriate microstructures and selection of materials with suitable modulus in flexible pressure sensors, which are potentially useful in intelligent robots and health monitoring.

1. Introduction

With the rapid development of soft robotics, human-machine interfaces, and internet of things, high-performance flexible tactile sensors or electronic skins have gained increasing attention [1–3], and have been reported to be potentially useful in application scenarios such as tactile perception for robots [4], and pulse wave detection for human beings [5]. Piezo-capacitive flexible tactile sensors have advantages over other types of sensors for their low signal drift and simple device structure [6]. However, they often present limited sensitivity owing to the incompressibility of soft dielectrics. The sensitivity of capacitive-type flexible tactile sensors can be enhanced by introducing specially designed microstructures in dielectric or electrodes, together with the use of ionic liquid, forming nanoscale iontronic interfaces which present ultrahigh specific capacitance [7–12]. These strategies, on the other hand, cause dramatic nonlinearity of the capacitance-to-pressure response featured as remarkably decreasing sensitivity with increasing pressure [13], as well as a narrow pressure response range. The high linearity of response is of great significance to bypass the need of pressure-response calibration, and thus helps simplify the data processing system and the circuit design, as well as improves the response speed of the system [14]. Therefore, sensors with high linearity of response over a broad pressure range are strongly required for many application scenarios such as the manipulation tasks in robots, pressure detection in aerodynamics, and plantar pressure sensing in wearables [15,16], which are often operated at pressures far higher than 10 kPa.

* Corresponding author.
E-mail address: guocf@sustech.edu.cn (C.F. Guo).

https://doi.org/10.1016/j.scib.2021.02.019

Please cite this article as: P. Lu, L. Wang, P. Zhu et al., Iontronic pressure sensor with high sensitivity and linear response over a wide pressure range based on soft micropillared electrodes, Science Bulletin, https://doi.org/10.1016/j.scib.2021.02.019

Although some capacitive-type flexible pressure sensors with linear signal-to-pressure response have been reported, their sensitivity values are extremely low because such devices often apply a flat elastomeric dielectric layer [17,18], which is incompressible. Generally, for flexible pressure sensors, there exists a contradiction between linearity and sensitivity that is related to the specific structures used in existing sensors. Most sensors adopt a dielectric layer with mechanically stable microstructures including micropyramids, cones, and domes to improve sensitivity because these structures are more compressible than flat dielectric layers. However, such stable microstructures undergo structural stiffening and thereby cause decreasing sensitivity as pressure increases [7,8,11,19]. For a common capacitive-type sensor with microstructures, its capacitance (C) follows $C \sim \varepsilon s/d$, where ε is the dielectric constant of the dielectric sandwiched between electrodes, s is the effective device area, and d is the thickness of the dielectric. The response largely lies in the change in dielectric constant ε and thickness d, while area s can hardly be changed under compression and its effect on sensing is negligible. Upon loading, the relative change in both ε and d decreases with increasing pressure due to the limited compressibility and stiffening of the microstructures. As a result, the response is nonlinear to the applied pressure.

In recent years, iontronic capacitive pressure sensors which consist of two flexible electrodes sandwiching an ionic gel layer have been developed [20]. An electric double layer (EDL) behaving like a capacitor forms at the interface between the electrode and the ionic gel when a small voltage is applied. The EDL capacitance is determined by the interfacial contact area (A), says $C \sim A$, significantly different from the sensing mechanism of the common capacitive sensors mentioned above. Such iontronic sensors often have a significant nano-interfacial behavior for which charges (ions in the ionic gel, and electrons in the electrode) are separated at an atomic length scale of ~1 nm (d ~1 nm), leading to ultrahigh signal intensity a few orders of magnitude higher than that of commonly used direct capacitors, and thereby ultrahigh sensitivity [21]. Existing iontronic sensors, however, still suffer from nonlinear response determined by the microstructure used [8,13]. Therefore, designing a sensor that possesses high sensitivity and linear response over a broad pressure range remains a big challenge.

Here we report a flexible iontronic pressure sensor that employs a micropillared electrode sustaining against a layer of soft ionic gel, exhibiting both high linearity (correlation coefficient R^2 ~0.999) and high sensitivity (33.16 kPa^{-1}) over a wide pressure range of 12–176 kPa. Upon pressing, the micropillars undergo three stages of deformations: initial contact at very low pressures (0–6 kPa), pillar buckling as pressure goes beyond the stability limit (6–12 kPa), and post-buckling with pillars laying against the ionic gel at high pressures (12–176 kPa) in which a linear response is achieved. The high linearity lies in the subtle change in the interfacial contact area enabled by the matching in Young's modulus between the electrode and the gel, which well compensates the stiffening effect of the microstructures. In addition to the high linearity and high sensitivity, the sensors also perform well by exhibiting a low detection limit of 0.9 Pa, a fast response time of 9 ms, and high signal and structure stability when subjected to cycling for over 6000 times of compression/release at a peak pressure of 80 kPa, which is a representative pressure used in manipulation tasks. The sensor and its array have been demonstrated to be potentially useful in physiological signal detection, plantar pressure mapping, as well as robotic manipulation tasks, for which linear response over a wide pressure range is desired. This work shows that the synergy between microstructure deformation and modulus matching of materials in the sensor can help achieve high sensitivity and high linearity simultaneously, allowing for robotic applications and human health monitoring.

2. Experimental

2.1. Finite element analysis

The three-dimensional finite element analysis was performed using commercial package Abaqus/Standard 2017. Both the pillars and the ionic gel were modeled as incompressible neo-Hookean materials with Young's modulus of 1 and 5 MPa, respectively. In order to simulate the buckling instability, a standard perturbation analysis was first performed to extract the buckling mode, and then the first positive buckling mode is superimposed to the original geometry with an imperfection factor of 0.01. A dynamic explicit step was then conducted in which the contact area between the ionic gel and the pillars was exported as a function of pressure. The interfacial contact assumed no friction or penetration. Each incremental time was small enough to ensure that the kinetic energy of the system is much lower than the strain energy such that the results were independent of time.

2.2. Micro-nano fabrication of micropillared structures

The fabrication of the micropillared structures were divided into two stages: the fabrication of microhole array in a silicon wafer serving as a template for the pillars, and the molding of the polydimethylsiloxane (PDMS) micropillared structures. The microholes were created by photolithography plus catalytic etching [22]. First, a circular Au disc tetragonal array with each disc of 10 μm in diameter, 30 μm in spacing, and 16 nm in thickness was deposited on top of silicon by using conventional photolithographic process. Next, a microhole array of 50 μm deep was formed by metal assisted catalytic etching using the Au discs as the template. The hole array was then subject to plasma treatment (TS-PL05, DongXin Gao Ke Co., Ltd.) at 500 W for 5 min. Following that, a layer of 1*H*, 1*H*, 2*H*, 2*H* perfluorooctyltrichlorosilane (from Macklin) molecules was evaporated on the surface of the silicon wafer with the holes. The treated silicon wafer was then used as a template to make polycarbonate (PC, Dongguan Ling Mei New Materials Co., Ltd.) micropillars by using hot embossing. Mixture of Sylgard 184 base and curing agent (Dow Corning Co., Ltd.) at a weight ratio of 10:1 was then casted on the PC micropillared structure, and heated at 80 °C for 3 h, forming a PDMS stamp with microholes, and then peeled off, followed by surface modification by plasma-treatment at 500 W for 5 min and deposition of a monolayer of 1*H*, 1*H*, 2*H*, 2*H* perfluorooctyltrichlorosilane to help demold. Another layer of PDMS (with base to curing agent ratio of 5:1) was spin-coated on the treated PDMS template at 400 r/min for 1 min, and heated at 80 °C for 3 h. After PDMS was cured, it was peeled off from the PDMS template, forming well-aligned micropillars. A layer of Au film with a thickness of 100 nm was then deposited on the micropillared PDMS substrate serving as the bottom electrode. The fabrication is illustrated in Fig. S1 (online).

2.3. Preparation of ionic gel

The ionic gel used in this study includes two components: poly (vinylidene fluoride-hexafluoropropylene) (P(VDF-HFP)) as the polymer skeleton, 1-ethyl-3-methylimidazolium bis(trifluoromethylsulfonyl) acyl imine ([EMIM] [TFSI]) as the ionic liquid filled in the polymer network. P(VDF-HFP) granules were first dissolved in acetone with a mass ratio of P(VDF-HFP) to acetone of 1:10, and then the solution was stirred until it became clear. Next, the [EMIM] [TFSI] (with [EMIM] [TFSI] to P(VDF-HFP) ratio of 3:1) was added to the completely dissolved solution, stirred until the solution became clear. The prepared solution was finally

spin-coated to form a 30 μm thick film at 200 r/min for 60 s, and placed in a fume hood for acetone to be completely evaporated.

2.4. Fabrication of the sensor

The sensor consists of three layers: a layer of 100 nm thick Au electrode deposited on colorless polyimide (CPI) by using e-beam evaporation and cut into desired shapes using a laser beam, a layer of 30-μm-thick ionic gel, and a PDMS micropillared electrode coated with 100 nm Au film was also cut into a desired shape using a laser beam. The sensor was finally encapsulated using thin polyimide (PI) tapes. For the sealing, each of the two electrodes (with a representative area of 7 mm × 7 mm) was first separately attached on a piece of sealing PI tape (10 mm in width). Next, the dielectric layer with the same area as the electrodes was aligned between the two electrodes placed face to face, and gently pressed for ~10 s to encapsulate the multilayers.

2.5. Fabrication of plantar pressure array

The ethylene-vinyl acetate copolymer (EVA) foam board was cut into the shape of a 42-yard insole, and 23 sensors (7 mm × 7 mm in size) were separately placed on the foam board. The sensors were connected with silver wires that penetrated to the foam and were led out from the back. Conductive carbon cloth threads (from Shenzhen Meicheng Co., Ltd.) were used to connect with the silver wires for signal collection.

2.6. Characterization and measurements

The surface morphology of the micropillared structure electrode was characterized by using field-emission scanning electron microscopy (FE-SEM, TESCAN). The capacitance was measured using an LCR meter (E4980AL, KEYSIGHT) at a frequency of 10^3 Hz. The response time was measured using another LCR meter (E4981A, KEYSIGHT) at a frequency of 10^3 Hz, because of its higher test speed (down to 2.3 ms). A force gauge with a computer-controlled stage (XLD-20E, Jingkong Mechanical Testing Co., Ltd.) was used to apply and record the external pressure loaded on the sensor. The sensitivity test, response hysteresis test, and working stability of the sensor were measured using this facility. The bending test of the sensor was performed using a smart stretching tester (WS 150–100).

2.7. Experiments on human subjects

All experiments were conducted under approval from the Institutional Review Board at the Southern University of Science and Technology (protocol number: 20190007).

3. Results and discussion

3.1. Micropillars deformation and sensitivity analysis

The sensor consists of three layers: a planar top electrode of a CPI membrane coated with 100 nm Au, a layer of ionic gel using P(VDF-HFP) as the polymer skeleton and [EMIM] [TFSI] as the ionic liquid, and a bottom electrode employing a height-to-radius aspect ratio (10:1) micropillar array of PDMS coated with a thin layer of Au film (100 nm), as shown in the schematic and SEM image in Fig. 1a. The microstructured electrode plays a key role to the sensing performance of the sensor, and detailed morphology of the pillars can be seen in Fig. S2 (online), showing large area pillars with high uniformity. When the pillar aspect ratio is further increased (>10), spontaneous structural collapse and defects occur (Fig. S3 online) [23]. The capacitance of the gel-electrode interface with micropillars is determined by the interfacial contact area, for which tiny EDL capacitors connected in parallel are formed, that is, $C_{\text{bottom}} = \Sigma C_{\text{EDL}}^{\text{pillar}}$, where C_{bottom} represents capacitance of the whole bottom electrode, and $C_{\text{EDL}}^{\text{pillar}}$ represents interfacial capacitance of each pillar, as shown in Fig. 1b. By contrast, the other EDL interface between the ionic gel and the planar electrode keeps unchanged upon loading because of the full contact, which is connected in series with the micropillared capacitance. As the top capacitance is far larger than that of the pillars, the total capacitance can be roughly expressed as $C \sim C_{\text{bottom}}$, determined by the pillar deformation. Fig. 1c shows a photograph of the sensor, which is 10 mm × 10 mm in area. Detailed fabrication procedure of the sensor is described in Experimental.

As an important parameter of the sensor, sensitivity is defined as $S = \delta(\Delta C/C_0)/\delta P$, where C_0 and ΔC are the initial capacitance before loading and the change in capacitance when loaded with a pressure P, respectively, and C_0 is determined to be 248 pF/cm^2. The sensor exhibits a sensitivity of 7.49 kPa^{-1} at the initial stage (P < 6 kPa), and 17.76 kPa^{-1} as pressure falls in the range of 6–12 kPa. As pressure further increases, sensitivity increases to 33.16 kPa^{-1} over a wide pressure range of 12–176 kPa, and the signal exhibits an excellent linearity with a high correlation coefficient (R^2) of 0.999 (Fig. 1d). At pressures higher than 180 kPa, ionic liquid might be partially squeezed out from the gel, leading to unstable signal, and thus the applied pressure is controlled to be below 180 kPa in our test. The three-phased response is found to result from the evolution in deformation modes of the micropillars from low to high pressures, denoted as Stage I, II, and III. Stage I features the initial contact of the pillars with the ionic gel before the onset of pillar buckling, exhibiting the lowest sensitivity and this state has been observed in our SEM inspection (Fig. 1e). As pressure increases, the pillar-gel interface transforms from the direct contact mode to a buckling mode (Fig. 1f) in the pressure range from 6 to 12 kPa, denoted as Stage II for which the side surface of the pillars makes direct contact with the ionic gel to form increasing EDL interfacial contact area, and sensitivity increases to a moderate value of 17.76 kPa^{-1} accordingly. The transition from Stage I to Stage II can be explained by the Euler's formula (Eq. (1)) [24,25], which depicts the critical compressive load that triggers the buckling instability of a long pillar.

$$\sigma_{\text{cr}} = \frac{\pi^2 E I_{\min}}{(\mu l)^2 A_{\text{c}}}, \tag{1}$$

where σ_{cr} is the critical stress causing pillar buckling, E is the Young's modulus, $I_{\min}$ is the minimum moment of inertia of the cross section of the pillar, and μ, l, and A_{c} are the length factor (μ = 2 in the clamped-free configuration, see Fig. S4 online), pillar height, and cross-sectional area of the pillars, respectively. For a pillar with a circular cross section, $I_{\min} = \pi r^4/4$, $A_{\text{c}} = \pi r^2$, and the critial stress can be expressed as

$$\sigma_{\text{cr}} = \frac{\pi^2 E r^2}{16 l^2} = \frac{\pi^2 E}{16 \lambda^2}, \tag{2}$$

where λ is the aspect ratio of the pillars ($\lambda = l/r$). From Eq. (2), σ_{cr} is inversely proportional to λ^2. That is, the higher aspect ratio the micropillars have, the smaller their destabilizing critical stress will be. Taking the modulus of ~1 MPa for PDMS pillars to the fomula (Fig. S5 online), σ_{cr} is determined to be 6.2 kPa, which agrees remarkably well with our experimental result. In Stage II (pressure between 6 and 12 kPa), buckling of the micropillars occurs. The deformation of the buckled micropillars upon loading is intuitively reflected in both our SEM observation and finite elemental analysis (FEA) results (Fig. S6 online). As pressure further increases to higher than 12 kPa, the buckled pillars lie down with their long axis being

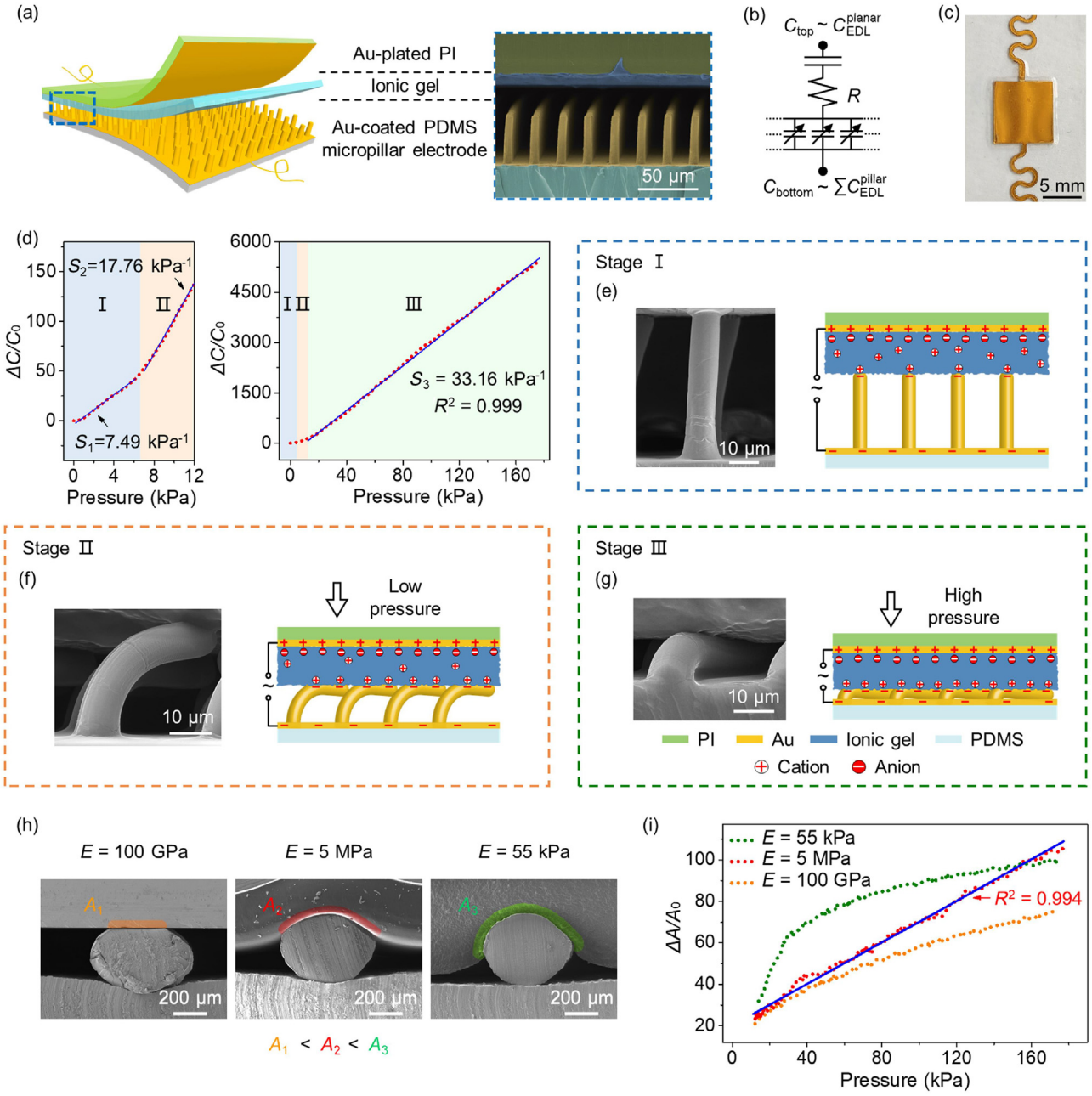

Fig. 1. (Color online) Sensor structure and three-staged sensing behavior. (a) Schematic illustration and cross-sectional view SEM image of micropillared structure iontronic pressure sensor. (b) Equivalent circuit of the sensor. (c) Photograph of the iontronic pressure sensor. (d) Change in capacitance as a function of pressure in a pressure range of 0–180 kPa. (e, f) Cross-sectional view SEM image of a micropillar and schematic illustration of the sensor structure (e) in initial status (Stage I) and (f) in the state of pillar buckling (Stage II). (g) Cross-sectional view SEM image of the collapsed micropillar and schematic illustration of the EDL of the collapsed micropillars under high pressure (Stage III). (h) Cross-sectional view SEM images of the interfaces between collapsed pillars and top materials of high (~100 GPa), medium (~5 MPa), and low rigidity (~55 kPa), showing that contact area significantly increases with decreasing rigidity. Applied pressure decreases from the left to right cases. (i) Normalized contact area as a function of applied pressure using finite elemental analysis (FEA) simulation. Young's moduli of the top layer are set to 100 GPa, 5 MPa, and 55 kPa.

parallel to the film plane (Fig. 1g), corresponding to Stage III which has a highly linear response.

The high linearity of the signal in Stage III lies in the synergy of structure deformation as well as the modulus matching between the ionic gel and the micropillars. First, microstructures upon loading often undergo structural stiffening, and thus sensitivity significantly decreases with increasing pressures. Such nonlinearity has been commonly seen in existing e-skins or flexible pressure sensors [7,11,13]. Second, the interfacial contact area is highly related to the Young's modulus of the top layer (gel). Typically, the interfacial contact area A increases as the top layer becomes softer. When the top layer is stiff, the incompressibility as well as the stiffening effect of the PDMS pillars will lead to saturation in contact area, and thus the sensitivity will decrease with increasing pressure. Here for our materials system, the ionic gel has a moderate Young's modulus of 5 MPa, which allows the PDMS pillars (Young's modulus: ~1 MPa) to partially embed into the gel to form extra contact upon loading, and the embedment subtly compensates the saturation effect mentioned above, leading to linear response. However, if the ionic gel is too soft (much softer than the PDMS pillars), excessive embedment may occur, causing significantly increased contact area as a result of full embedment in the

low-pressure regime and thereby nonlinearity in response. The effect of the Young's modulus of the top layer (e.g., 55 kPa, 5 MPa, and 100 GPa) on contact area has been verified in our SEM observation and FEA as shown in Fig. 1h and i, respectively. The embedment of the micropillar into soft top layers (5 MPa and 55 kPa) upon loading is confirmed in our SEM observation. By contrast, the stiff top layer (~100 GPa) shows no dent, but significantly squashes the micropillar with limited interfacial contact area (A). We can clearly see that the interfacial contact area increases with the decreasing modulus of the top layer. That is, $A_1 < A_2 < A_3$, here A_1, A_2, A_3 correspond to the contact area of the pillar and the top layer with a Young's modulus of ~100 GPa, 5 MPa, and 55 kPa, respectively. We also provide detailed contour plots and video (Movies S1–S3, and Figs. S7, S8 online) to show the change in interfacial contact as pressure increases. Our FEA simulation clearly suggests that our selection of 5 MPa leads to a remarkable linearity (R^2 ~0.994), whereas others (with either higher or lower rigidity) show significant nonlinearity. Our results illustrate a principle: although the deformation of surface microstructures is often nonlinear to applied pressure, the interfacial contact area can still be made linear to the load by coupling with a soft material that has a moderate rigidity.

3.2. Sensing properties of the sensor

Some other sensing properties are also enhanced by our structural design. The extremely small initial contact area and the high specific capacitance of the ionic gel make the sensor highly sensitive to weak mechanical stimuli, and thus the sensor exhibits a low limit of detection (LOD) of 0.9 Pa (Fig. 2a), which is significantly lower than that of the human skin (~1 kPa) [26]. During a loading/release cycle, micropillars undergo deformation and structural recovery, greatly reducing the viscoelasticity of the interface. This is because there are a lot of voids and air gaps formed at the electrode-gel interface, enabling the microstructures to deform elastically. The microstructures can quickly store and release energy to help the interface deform and recover elastically, thereby minimizing the hysteresis caused by viscoelasticity [7]. As a result, the sensor exhibits high response and relaxation speed of 9 ms (Fig. 2b), much faster than that of the human skin (30–50 ms), and fast enough for a variety of robotic and wearable applications [27]. Because of the high structural elasticity, the hysteresis effect of the sensor is negligible (Fig. 2c).

The stability of the sensor over long-term and cyclic loading/unloading is critical to its real applications. Two aspects-sensing performance stability and structure stability over cycling need to be assessed. The sensor is first subjected to repeated compression/release under a peak pressure of 80 kPa for over 6000 cycles, showing no significant signal drift or fatigue (Fig. 2d). The low drift and low fatigue of the signal result from the high stability of the microstructures. Each micropillar has a PDMS core with an ultrathin layer of Au film (~9 nm) coated on the surface, and all pillars fully recover to the initial state after the pressure is removed (Fig. 2e and f). As a result, no cracks are formed during pillar bending (Fig. S6 online). The thickness of the Au film can be figured out based on the wavelength of the surface wrinkles on the pillars (Fig. S9 online) [28]. Although folding and cracking of the Au film occur on the planar surface of the PDMS substrate as verified by our SEM observation (Fig. 2f), those imperfections have little influence on the electrical properties of the electrode due to delocalized rupture that results in fine and distributed slits [29,30]. The Au film with cracks is still well-interconnected. We tested the stability of the resistance of the micropillared electrode with an area of 10 mm × 10 mm over 6000 compression/releasing cycles to a high pressure of 160 kPa (which is close the highest pressure allowed), and little increase (~11%, from 10.2 to 11.2 Ω) was found (Fig. 2g). Since capacitance is not sensitive to the resistance of electrodes, such a small change in resistance does not cause any capacitance signal drift or fatigue. In addition, the high chemical stability, high ductility, and high electrical conductance of Au also contribute to the high stability of the sensor, although Au is expensive compared with many other metals.

The sensor is further tested under different bending radii and cyclic bends to investigate its stability in different mechanical conditions. For the bending test, the capacitance of the sensor increases with the decreasing of the bending radius (Fig. 2h), which can be reasonably attributed to the increasing compressive pressure applied on the pillars at lower bending radii. In addition, the sensor exhibits no change in signal amplitude over 6000 bending/release cycles with a minimal radius of curvature of 13 mm (Fig. 2i). As such, the sensor is expected to be applied to test joint motions of the human body, being potentially useful for movement monitoring in wearables.

In view of that environmental change may affect sensing properties in practical applications, the sensor is subject to different relative humidity to measure its signal stability. Although the ionic gel is sensitive to humidity, the signal does not change significantly with the change in relative humidity from 40% to 80% (Fig. S10 online) because the sensor is tightly sealed using thin PI tapes, guaranteeing the performance stability of the sensor under different humidity and human body conditions (e.g., sweating). The sealing, on the other hand, will introduce a pre-pressure to the sensor, which leads to increased initial capacitance and decreased sensitivity. Nevertheless, the sensor's capability to distinguish pressure as well as the linearity will not be affected, especially in Stage III.

3.3. Highly linear response and applications of the sensors

Sensors with high sensitivity and a wide linear response range can accurately collect pressure information at different base pressures over a wide range, which is desired in the applications of tactile perception for humanoid robots, physiological signal detection for human body, and human-computer interaction [14,15]. Fig. 3 compares our sensor with three types of other sensors that apply stable microstructures or a flat device structure in terms of sensitivity, linearity, and pressure response range. Whereas our sensor has a superior balance on these sensing parameters, existing sensors significantly underperform in at least one of the three aspects. Iontronic sensors with stable microstructured ionic gels or electrodes (micropyramids, domes, etc.) are often highly sensitive at low pressures (S > 10 kPa^{-1}). However, their sensitivity decreases significantly with increasing pressure, and often drops to a value lower than 1 kPa^{-1} as pressure goes higher than 50 kPa [8,13]. Likewise, non-iontronic sensors with microstructures also exhibit a decreasing sensitivity as pressure increases but their sensitivity values are much lower than that of the iontronic type [31–35]. For non-iontronic capacitive pressure sensors with a flat dielectric and electrodes, their sensitivity is linear but extremely low (~0.01 kPa^{-1}) over a wide pressure range [35], which is at least three orders of magnitude lower than the sensitivity of our sensor over full scale, and thus incompetent for many practical applications.

With superior overall performances, here in this work we conducted a test of our sensor to mimic pressure sensing in real applications to demonstrate its linear sensing performance over a wide pressure range. Stepped pressures from ~64 to ~164 kPa with a pressure increment of ~20 kPa were applied on the sensor, and the measured capacitance was found to respond steppedly and linearly with the increase of pressure (Fig. 4a). We also designed experiments to prove that the sensor can maintain a linear response in real application scenarios by resolving small pressure changes under a high base-pressure. A heavy block that generates

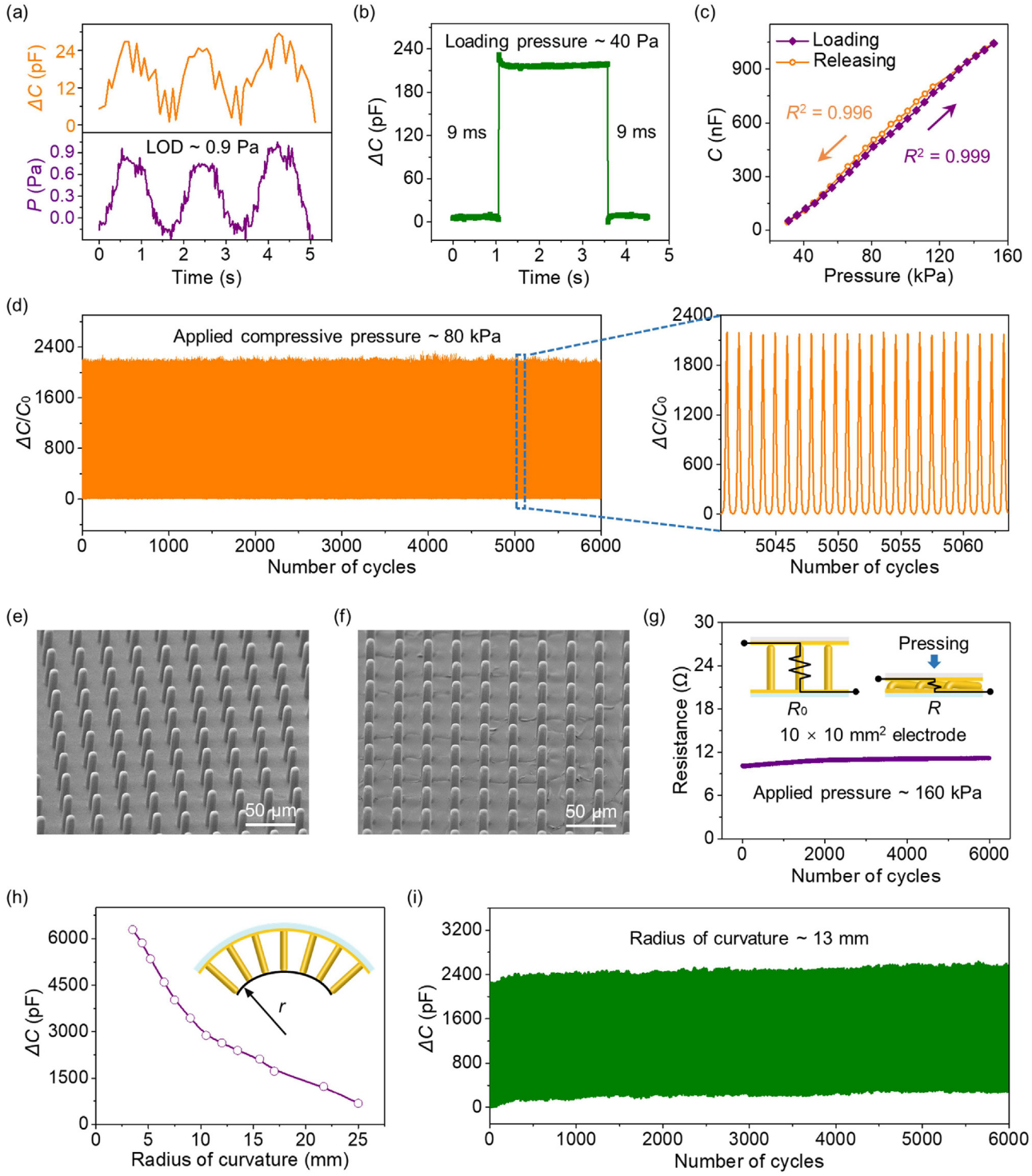

Fig. 2. (Color online) Sensing properties of the micropillared iontronic pressure sensor. (a) Limit of detection (LOD). (b) Response and relaxation speed. (c) Response hysteresis. (d) Working stability of the sensor tested over 6000 cycles under a pressure of 80 kPa. (e, f) The 45° tilt-view SEM images of the micropillared structure electrode (e) before and (f) after repeated loading/unloading. (g) Stability in resistance of the micropillared electrode under cyclic loading to 160 kPa. (h) Change in capacitance as a function of bending radius. (i) Response over 6000 cycles of bending/releasing at a bending radius of ~13 mm.

a high base-pressure of 160 kPa was placed on a sensor, and five standard nuts, each with a weight of 2 g producing 0.43 kPa pressure, were then added on the block in sequence. As we put the nuts on the block one by one (Fig. 4b), the sensor exhibited uniformly stepped capacitance increase with a response speed of ~100 ms as the nuts are added (Fig. 4c). This experiment shows that the sensor can still accurately sense small objects with high linearity under high base-pressures, but with a lower response speed.

The human hand can distinguish the relative weight of objects with the help of a tremendous of tactile receptors distributed in the skin. Here we laminated a single sensor (2 mm × 6 mm in size) on the middle finger segment of an artificial hand to mimic the function of weighting of human hand. A paper cup was hung on the sensor with four pieces of plastic belts of ~10 cm long, and weights of different values were then added into the cup (Fig. 4d). A weight of 300 g was first put into to stabilize the cup.

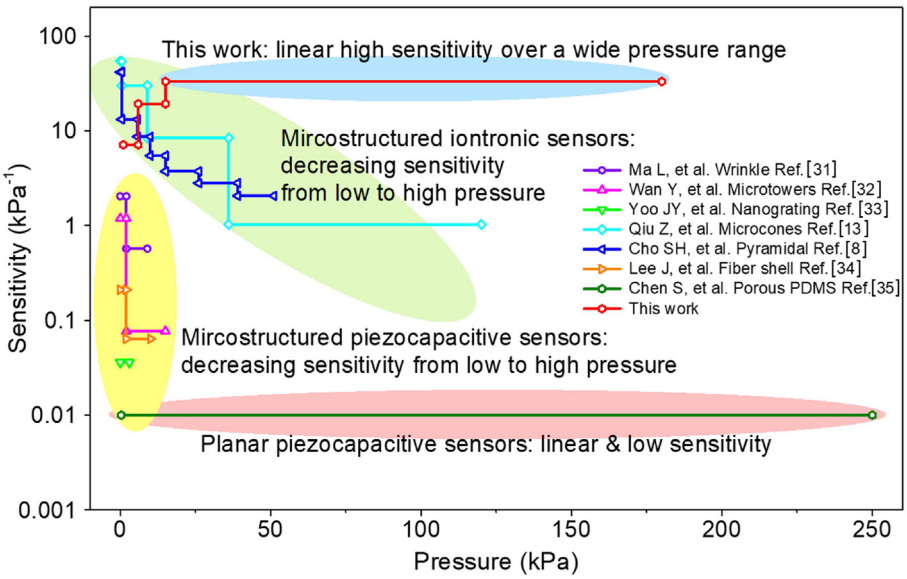

Fig. 3. (Color online) Comparison of sensitivity of our pressure sensor with other capacitive sensors that employ stable surface microstructures or planar structures.

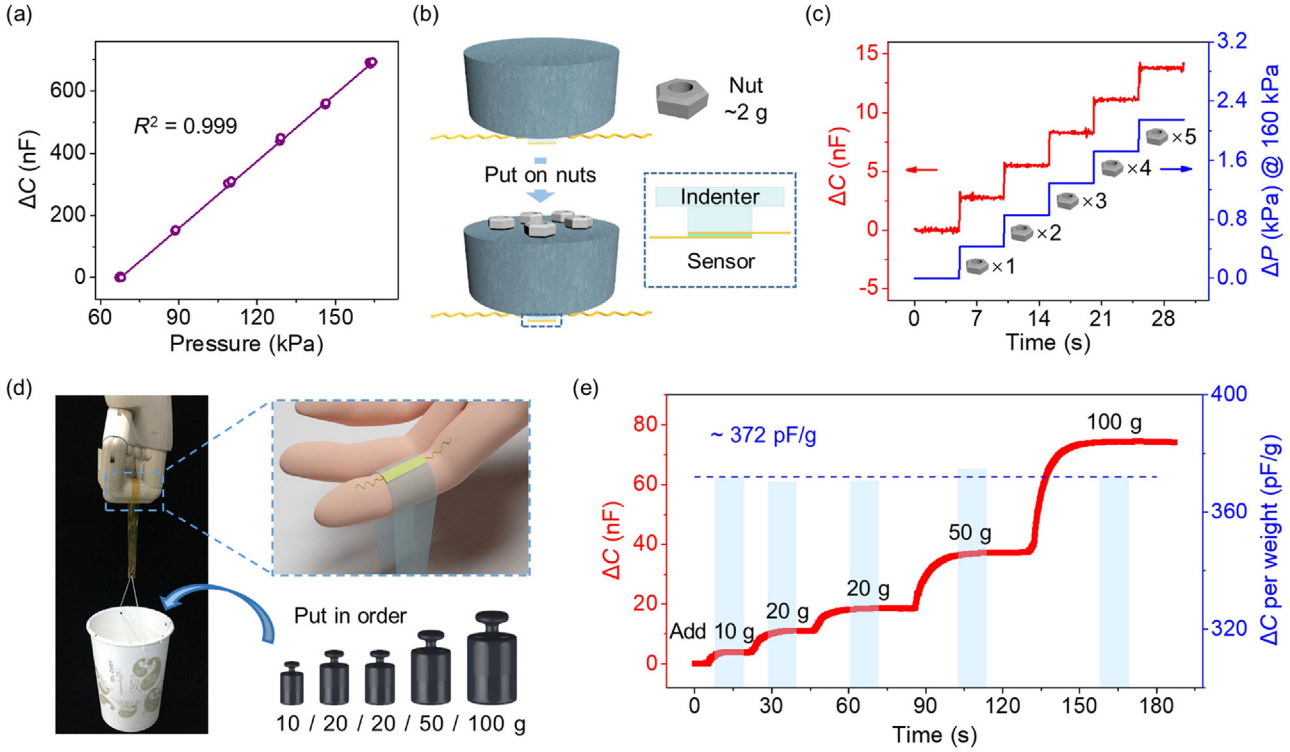

Fig. 4. (Color online) Linear response of the micropillared iontronic pressure sensor. (a) Change in capacitance as a function of stepped increment of pressure (~20 kPa) from 64 to 164 kPa, showing high linearity over a wide pressure range. (b, c) Detection of small objects (nut that weighs 2 g) under a 160 kPa base-pressure, showing that the capacitance increases steppedly and linearly with when loading the nuts in sequence. (d) Sensor attached on a finger of an artificial hand for mimicking the weighting function of human hand. (e) Capacitance signals corresponding to the added weight in the paper cup.

Next, weights of 10, 20, 20, 50, and 100 g were added into the cup in sequence and capacitance as a function of time was recorded. As shown in Fig. 4e, the capacitance is in proportion to the increasing weight with a rate of ~372 pF/g, but it takes a few seconds for the signal to get stabilized because the cup is hung with long plastic belts. The sensor is therefore expected to endow artificial hands with a weighting function, which is an important application for humanoid robots.

We have also applied our sensor in physiological signal monitoring, plantar pressure mapping, and robotic manipulation, to show its potential in a variety of applications including healthcare, motion detection, as well as intelligent robotics. The radial artery pulse is important physiological information that can well reflect the cardiological health conditions of human beings. We put a sensor of 5 mm × 5 mm in area on the radial artery skin surface of a male subject (Fig. 5a) and recorded its capacitance signals at

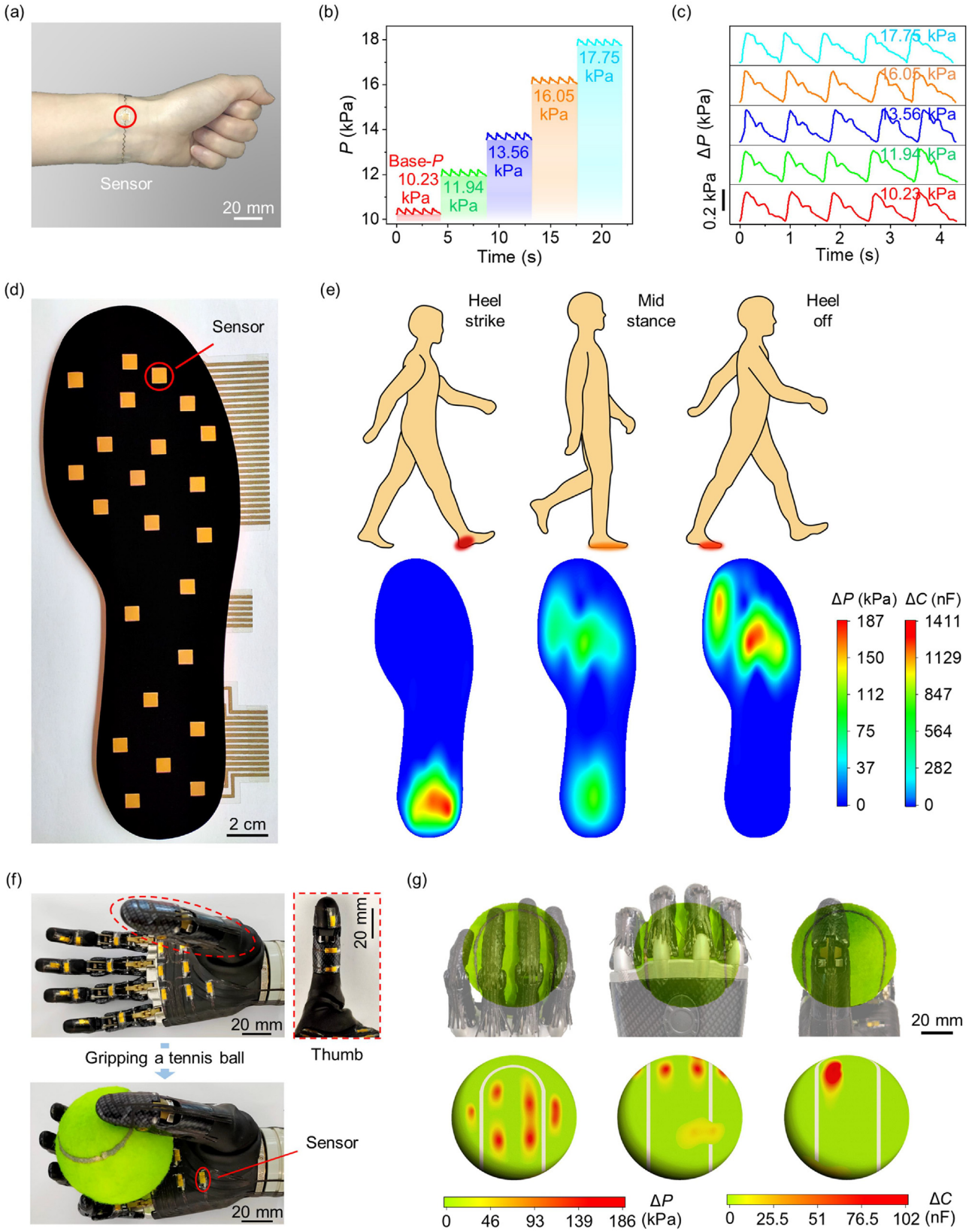

Fig. 5. (Color online) Sensor applications. (a) Measurement of radial artery pulse waveform using a 5 mm × 5 mm sensor. (b, c) By applying different base-pressures, the intensity of radial artery pulse signals keep relatively stable. (d) Photograph of a plantar pressure sensor array. (e) Schematic illustrations of three gaits during walking, and the capture of the capacitance signals of the three gaits by using the sensor array. (f) Sensors laminated on the surface of an artificial hand, and a photograph of gripping task of a tennis ball with the artificial hand. (g) Three-dimensional pressure distributions of the ball at three different angles.

different base pressures (Fig. 5b). We can see that pulse wave can be well detected with the base pressure increasing from 10.23 to 17.75 kPa, and little change in signal amplitude was found with increasing pressures (Fig. 5c). Typically, each pulse exhibits two distinct contraction peaks P_1 and P_2 resulting from the early systolic spike in blood ejection and blood flow reflection, respectively [36]. In addition, the pulse augmentation index (*AIr*) is an important parameter that reflects the degree of vascular sclerosis [37], defined as the ratio between the amplitude of P_2 and P_1 [36], and the parameter ΔT_{DVP} represents the time interval between the two peaks [5]. In our study, the tested pulse wave exhibits an *AIr* value of 61.1% and a ΔT_{DVP} of 273 ms, all falling in the normal ranges (Fig. S11 online). Such data could preliminarily help assess and conclude that the subject does not suffer from an atherosclerosis. It shows that the sensor can well detect human pulse waveform, indicating its potential of being applied in advanced healthcare.

We further made an array of sensors for pressure mapping to judge the shape of the object loaded on the sensor array. The sensor array has 6 × 6 pixels with each sensing element being 2 mm × 2 mm in size and gaps between the sensing elements being also 2 mm. The sensor array could accurately detect the contour of the applied weight or pressure distribution caused by the weight (Fig. S12a online), and also clearly respond to more complex objects, exemplified by the one in the shape of "5" that applies a 0.7 N force or a 10.3 kPa pressure (Fig. S12b online). The result also shows that the sensor array is capable of resolving pressure with a millimeter spatial resolution (~4 mm). Higher spatial resolution is expected but has not yet been demonstrated in this study.

The plantar pressure distribution is essential to assess the dynamic loads during human body activities including walking. Here a sensor array is applied for the detection of plantar pressure distribution. A layer of EVA foam was cut into the shape of a 42-yard insole, being used as the substrate. Twenty-three sensors, each of 7 mm × 7 mm in area, were arranged in a non-matrix format in the toe, sole, arch, and heel positions (Fig. 5d). Silver threads connected to the sensors were deployed on the backside of the foam and then connected to carbon cloth threads for capacitance signal collection (Fig. S13 online). The pressure distributions of three gaits during walking including heel-strike, mid-stance, and heel-off were recorded (Fig. 5e). The difference in pressure distribution among the three different gaits can be clearly seen: the pressure concentrates on the center of the heel during heel-strike, and distributes uniformly on both the heel and the forefoot at the mid-stance state with a lower maximal pressure; for the posture of heel-off, the pressure mainly concentrates on the big toe and the forefoot. The accurate measurement of dynamic plantar pressure distributions is especially significant for professional athletes. Long-term overloading on foot may lead to stress fracture of the metatarsal bones, a commonly seen danger in athletes that may threaten their professional career [38]. Once a popular basketball player, YAO Ming, ended his career in this way at a young age. As such, shoes with such an insole that can dynamically and sensitively detect the pressure distribution of the foot over a wide pressure range would be of great interest in the shoemaking industry and the sports industry.

The high linearity of response with high sensitivity over a broad pressure range also plays an important role in the manipulation tasks of artificial limbs or grippers. Here in this work, we laminated 21 sensors, each with a size of 3 mm × 3 mm, on the palm and fingers of a commercial artificial limb to test the pressure distribution of the manipulated object. A tennis ball was used in the grasp task, and pressure for each sensing pixel was recorded as fingers were gripping the ball (Fig. 5f). The pressure distribution of the ball surface is illustrated in Fig. 5g, showing that pressures on the fingers are much higher than that on the palm. Specifically, the thumb generates the highest pressure during gripping. Such pressure information can be used to analyze the kinematic parameters in manipulation tasks, and in turn optimize the design of artificial limbs. The experiment also indicates that the sensors we designed might be used for tactile sensing in intelligent robotics.

4. Conclusion

In summary, we have designed an iontronic pressure sensor that has micropillared electrode with pillars placed against a layer of ionic gel to form an EDL interface. The sensor can dynamically and linearly respond to mechanical stimuli with a high sensitivity. Our experimental observation and FEA results illustrate that the micropillars undergo three stages of deformation upon loading: initial contact, pillar buckling, and post-buckling. In the post-buckling stage, the pillars are squashed and the gel-electrode interface is deflected, corresponding to the linear and highly sensitive response (S ~ 33.16 kPa^{-1}) over a wide pressure range (12–176 kPa). The high linearity lies in the synergy between structural stiffening and contact area compensation at the electrode-gel interface determined by mechanical matching. The linear response and wide pressure response range of our sensor enables a few application scenarios, such as stable pulse detection at changing base-pressures, plantar pressure mapping under different gaits, and robotic manipulation. This work offers a physical insight on the deformation mode and sensing mechanism of unstable micropillar structures that are used for providing high linearity of response for sensors. Our sensor is expected to have potential applications where high sensing linearity over a broad pressure range is required, not only limited to the demonstrations in this work.

Conflict of interest

The authors declare that they have no conflict of interest.

Acknowledgments

This work was supported by the Science Technology and Innovation Committee of Shenzhen Municipality (JCYJ20170817111714314), the National Natural Science Foundation of China (52073138 and 51771089), the Guangdong Innovative and Entrepreneurial Research Team Program (2016ZT06G587), the Shenzhen Sci-Tech Fund (KYTDPT20181011104007), and the Tencent Robotics X Lab Rhino-Bird Focused Research Program (JR201984).

Author contributions

C. F. Guo conceived the idea and designed the experiments. P. L. conducted the majority of experiments. L. W. did the FEA simulation. P. Z., Y. W. and K. Xie participated in sample fabrication. J. H., Y. W., N. B. and Y. D. contributed to the general discussion. G. L., J. Y., J. Z. and B. Y. helped with the materials characterizations. The manuscript was written through contributions of all authors.

Appendix A. Supplementary materials

Supplementary materials to this article can be found online at https://doi.org/10.1016/j.scib.2021.02.019.

References

[1] Hammock ML, Chortos A, Tee BC, et al. 25th Anniversary article: the evolution of electronic skin (e-skin): a brief history, design considerations, and recent progress. Adv Mater 2013;25:5997–6038.

[2] Wan Y, Wang Y, Guo CF. Recent progresses on flexible tactile sensors. Mater Today Phys 2017;1:61–73.
[3] Huang Y, Fan X, Chen SC, et al. Emerging technologies of flexible pressure sensors: materials, modeling, devices, and manufacturing. Adv Funct Mater 2019;29:1808509.
[4] Guo Y, Guo Z, Zhong M, et al. A flexible wearable pressure sensor with bioinspired microcrack and interlocking for full-range human-machine interfacing. Small 2018;14:1803018.
[5] Lee YH, Kweon OY, Kim H, et al. Recent advances in organic sensors for health self-monitoring systems. J Mater Chem C 2018;6:8569–612.
[6] Zang Y, Zhang F, Di C, et al. Advances of flexible pressure sensors toward artificial intelligence and health care applications. Mater Horiz 2015;2:140–56.
[7] Mannsfeld SC, Tee BC, Stoltenberg RM, et al. Highly sensitive flexible pressure sensors with microstructured rubber dielectric layers. Nat Mater 2010;9:859–64.
[8] Cho SH, Lee SW, Yu S, et al. Micropatterned pyramidal ionic gels for sensing broad-range pressures with high sensitivity. ACS Appl Mater Interfaces 2017;9:10128–35.
[9] Yang J, Luo S, Zhou X, et al. Flexible, tunable, and ultrasensitive capacitive pressure sensor with microconformal graphene electrodes. ACS Appl Mater Interfaces 2019;11:14997–5006.
[10] Chhetry A, Yoon H, Park JY. A flexible and highly sensitive capacitive pressure sensor based on conductive fibers with a microporous dielectric for wearable electronics. J Mater Chem C 2017;5:10068–76.
[11] Wan Y, Qiu Z, Huang J, et al. Natural plant materials as dielectric layer for highly sensitive flexible electronic skin. Small 2018;14:1801657.
[12] Zhu Z, Li R, Pan T. Imperceptible epidermal–iontronic interface for wearable sensing. Adv Mater 2018;30:1–9.
[13] Qiu Z, Wan Y, Zhou W, et al. Ionic skin with biomimetic dielectric layer templated from calathea zebrine leaf. Adv Funct Mater 2018;28:1802343.
[14] Hille P, Höhler R, Strack H. A linearisation and compensation method for integrated sensors. Sens Actuators A 1994;44:95–102.
[15] Wang X, Dong L, Zhang H, et al. Recent progress in electronic skin. Adv Sci 2015;2:1500169.
[16] Wang C, Hwang D, Yu Z, et al. User-interactive electronic skin for instantaneous pressure visualization. Nat Mater 2013;12:899–904.
[17] Yin XY, Zhang Y, Cai X, et al. 3D printing of ionic conductors for high-sensitivity wearable sensors. Mater Horiz 2019;6:767–80.
[18] Shao R, Wang C, Wang G, et al. A highly accurate, stretchable touchpad for robust, linear, and stable tactile feedback. Adv Mater Technol 2020;5:1900864.
[19] Park J, Kim J, Hong J, et al. Tailoring force sensitivity and selectivity by microstructure engineering of multidirectional electronic skins. NPG Asia Mater 2018;10:163–76.
[20] Nie B, Xing S, Brandt JD, et al. Droplet-based interfacial capacitive sensing. Lab Chip 2012;12:1110–8.
[21] Tang Z, Scriven LE, Davis HT. A three-component model of the electrical double layer. J Chem Phys 1992;97:494–503.
[22] Lai RA, Hymel TM, Narasimhan VK, et al. Schottky barrier catalysis mechanism in metal-assisted chemical etching of silicon. ACS Appl Mater Interfaces 2016;8:8875–9.
[23] Zhang Y, Lo CW, Taylor JA, et al. Replica molding of high-aspect-ratio polymeric nanopillar arrays with high fidelity. Langmuir 2006;22:8595–601.
[24] Sadowsky MA, Pu SL, Hussain MA. Buckling of microfibers. J Appl Mech 1967;34:1011–6.
[25] Kuzkin VA, Dannert MM. Buckling of a column under a constant speed compression: a dynamic correction to the Euler formula. Acta Mech 2016;227:1645–52.
[26] Johansson RS, Flanagan JR. Coding and use of tactile signals from the fingertips in object manipulation tasks. Nat Rev Neurosci 2009;10:345–59.
[27] Boutry CM, Nguyen A, Lawal QO, et al. A sensitive and biodegradable pressure sensor array for cardiovascular monitoring. Adv Mater 2015;27:6954–61.
[28] Huck WT. Hierarchical wrinkling. Nat Mater 2005;4:271–2.
[29] Guo CF, Sun T, Liu Q, et al. Highly stretchable and transparent nanomesh electrodes made by grain boundary lithography. Nat Commun 2014;5:3121.
[30] Lacour SP, Chan D, Wagner S, et al. Mechanisms of reversible stretchability of thin metal films on elastomeric substrates. Appl Phys Lett 2006;88:204103.
[31] Ma L, Shuai X, Hu Y, et al. A highly sensitive and flexible capacitive pressure sensor based on a micro-arrayed polydimethylsiloxane dielectric layer. J Mater Chem C 2018;6:13232–40.
[32] Wan Y, Qiu Z, Hong Y, et al. A highly sensitive flexible capacitive tactile sensor with sparse and high-aspect-ratio microstructures. Adv Electron Mater 2018;4:1700586.
[33] Yoo JY, Seo MH, Lee JS, et al. Industrial grade, bending-insensitive, transparent nanoforce touch sensor via enhanced percolation effect in a hierarchical nanocomposite film. Adv Funct Mater 2018;28:1804721.
[34] Lee J, Kwon H, Seo J, et al. Conductive fiber-based ultrasensitive textile pressure sensor for wearable electronics. Adv Mater 2015;27:2433–9.
[35] Chen S, Zhuo B, Guo X. Large area one-step facile processing of microstructured elastomeric dielectric film for high sensitivity and durable sensing over wide pressure range. ACS Appl Mater Interfaces 2016;8:20364–70.
[36] Chirinos JA, Kips JG, Roman MJ, et al. Ethnic differences in arterial wave reflections and normative equations for augmentation index. Hypertension 2011;57:1108–16.
[37] Kohara K, Tabara Y, Oshiumi A, et al. Radial augmentation index: a useful and easily obtainable parameter for vascular aging. Am J Hypertens 2005;18:11S–4S.
[38] Tao W, Liu T, Zheng R, et al. Gait analysis using wearable sensors. Sensors 2012;12:2255–83.

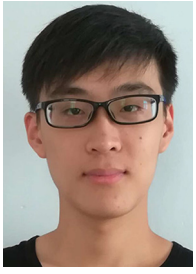

Peng Lu is a research assistant in the Department of Materials Science & Engineering, Southern University of Science and Technology (SUSTech). He received a joint M.S. degree in Materials Engineering of SUSTech and Harbin Institute of Technology. His research interest focuses on the flexible electronic skins.

Chuan Fei Guo is an associate professor in the Department of Materials Science & Engineering, SUSTech. He received his Ph.D. degree in Condensed Matter Physics from the National Center for Nanoscience and Technology (NCNST), Chinese Academy of Sciences, China. From 2011 to 2016, he worked as a postdoctoral fellow and research associate at Boston College and the University of Houston. His research interest focuses on the flexible electronics and advanced manufacturing.